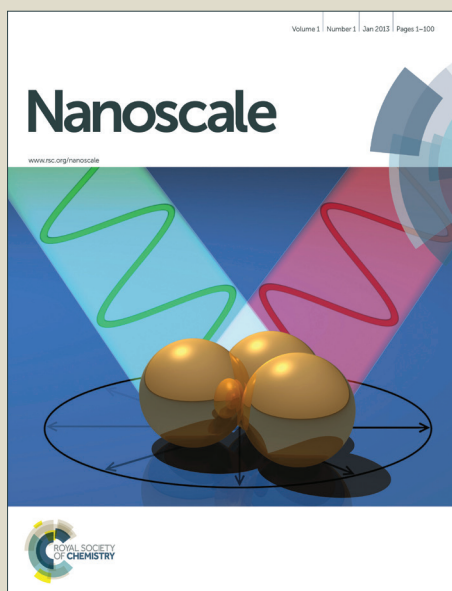


Nanoscale

Accepted Manuscript



This is an *Accepted Manuscript*, which has been through the Royal Society of Chemistry peer review process and has been accepted for publication.

Accepted Manuscripts are published online shortly after acceptance, before technical editing, formatting and proof reading. Using this free service, authors can make their results available to the community, in citable form, before we publish the edited article. We will replace this *Accepted Manuscript* with the edited and formatted *Advance Article* as soon as it is available.

You can find more information about *Accepted Manuscripts* in the [Information for Authors](#).

Please note that technical editing may introduce minor changes to the text and/or graphics, which may alter content. The journal's standard [Terms & Conditions](#) and the [Ethical guidelines](#) still apply. In no event shall the Royal Society of Chemistry be held responsible for any errors or omissions in this *Accepted Manuscript* or any consequences arising from the use of any information it contains.

COMMUNICATION

Metal nanocluster light-emitting devices with suppressed parasitic emission and improved efficiency: Exploring the impact of photophysical properties

Cite this: DOI: 10.1039/x0xx00000x

Received 00th January 2012,
Accepted 00th January 2012T. -W. Koh,^a A. M. Hiszpanski,^b M. Sezen,^b A. Naim,^c T. Galfsky,^c A. Trivedi,^d Y. -
L. Loo,^b V. Menon^c and B. P. Rand^{a,c}

DOI: 10.1039/x0xx00000x

www.rsc.org/

Here we investigate photophysical properties of Au(0)@Au(I)-thiolate nanoclusters by controlling the degree of aggregation, and measure electrochemical energy levels to design a metal nanocluster-based thin film LED (MNC-LED) structure. These efforts allow us to implement the very first MNC-LEDs with luminance exceeding 40 cd m⁻² and external quantum efficiency exceeding 0.1% with clearly visible orange emission. It is also demonstrated that by varying the sizes of nanoclusters, electroluminescence spectrum of the device can be tuned to infrared emission, indicating the possibility of exploiting metal nanocluster emitters for use over a wide spectral range.

Introduction

Thin film light-emitting devices (LEDs) have the potential to significantly change both the lighting and display industries, owing to their ability to adapt to various form factors without having to sacrifice high device efficiency. Organic LEDs (OLEDs) are of particular interest owing to their unique characteristics such as areal emission, their ability to be made flexible and/or semi-transparent,¹⁻³ and their compatibility with diverse types of substrates (e.g. metal foils,⁴ plastic substrates,⁵ paper⁶), each of which allow for electronic devices with an unprecedented degree of freedom in design. Organic molecular emitters used in OLEDs are known for their excellent photoluminescence quantum yields, exceeding 90% for certain phosphorescent emitters,^{7,8} and well-established device structures. However, there remain unresolved issues in these molecular emitters, for instance complicated synthetic protocols that compromise yield and increase cost, moderate color purity,⁹ and short operational lifetime of blue phosphorescent dopants in particular.¹⁰ In an effort to resolve these issues, new types of emitters

have been actively investigated. One that has received particular attention is the semiconductor quantum dot (QD) in which carefully designed core-shell structures lead to a quantum confinement effect that enables luminescence from the excited states in these quantum dots. Demonstrations of using QDs as active emitters in thin film LEDs has proven to be highly successful, with recent reports achieving external quantum efficiencies (EQE) of approximately 20%.^{11,12} While state-of-the-art QDs have many advantages over molecular emitters such as narrow, highly saturated,¹³ and tunable emission color depending on the degree of control over QD size dispersion¹⁴ and choice of core and shell materials,¹⁵ some of their drawbacks include relatively high volume-to-surface ratio hindering efficient Förster or direct charge transfer to emissive sites,¹⁶ complicated and costly fabrication processes,¹⁷ and the use of toxic heavy metals.¹⁸

For these reasons, we are investigating the use of metal nanoclusters as active emitters in thin film LEDs, in which a 'core' is comprised of several tens of metal atoms and is surrounded by a 'shell' typically composed of organic ligands. Charge transfer between the core and shell (ligand-to-metal or ligand-to-metal-metal charge transfer) leads to effective absorption and re-emission of photons as shown in the previous work by Luo et al,¹⁹ opening up the possibility of using these nanoclusters as electroluminescent devices. Metal nanoclusters also possess unique merits such as small cluster volumes (diameter typically less than a few nanometers),²⁰ high photoluminescence quantum yield,²¹ nontoxicity which enable their use as biocompatible probes in living organs,²² and a highly scalable, cost-effective synthesis.²³ To the best of our knowledge, the first and only attempt to utilize metal nanoclusters within thin film LEDs was made by Niesen et al,²⁴ demonstrating that it is indeed possible to observe electroluminescence from a thin film of metal nanoclusters. However, the peak luminance of the device was under 1 cd m⁻². Furthermore, the device exhibited significant parasitic emission from the adjacent hole injection layer. Here we show a thin

film metal nanocluster LED with clearly visible orange emission with a peak luminance $>40 \text{ cd m}^{-2}$ without parasitic emission and tunable emission spectra according to the nanocluster sizes, all aspects of which were made possible by proper engineering of the nanoclusters and development of a device structure that allows for orders of magnitudes more efficient electroluminescence. These enhancements were achieved by a deeper understanding of the nanocluster characteristics by the means of photophysical analyses, including cyclic voltammetry for energy level measurement and transient photoluminescence lifetime measurement for understanding their spontaneous emission behavior.

Results and discussion

In order to pursue light-emitting devices with an improved efficiency compared to previous work,²⁴ it is important to begin with emitters with high photoluminescence quantum yields (PLQY). Thus, we have adopted a novel, one-pot-synthesized gold nanocluster structure proposed by Luo et al.,¹⁹ wherein Au(I)-thiolate complexes surround Au(0) cores. This aggregation-induced type of emission from gold nanoclusters has been shown to achieve a PLQY as high as 15%, while higher PLQY values have been reported for nanoclusters with different synthetic protocols and chemical structures.²⁵ The synthesis features two starting materials, hydrogen tetrachloroaurate trihydrate ($\text{HAuCl}_4 \cdot 3\text{H}_2\text{O}$) and L-Glutathione in the reduced form (GSH), that are mixed in water and subsequently selectively reduced and aggregated under heating/stirring (details in the experimental methods section). To control the size (and hence the degree of aggregation) of the clusters, we have varied the GSH: Au salt molar ratios as 1.2:1, 1.5:1, and 1.8:1, the lower molar ratios leading to smaller nanoclusters. As identifying buffer layers compatible with respect to orthogonality and wettability with the aqueous dispersion of nanoclusters was difficult, we have transferred the nanoclusters into toluene using CTAB (hexadecyltrimethyl ammonium bromide) as a phase transfer agent,²⁰ with a concentration half that of the original aqueous solution. The absorbance of these gold nanoclusters in toluene are shown in Figure 1(a) (inset images are the photos of these solutions under ambient light (top) and ultraviolet light (bottom)).

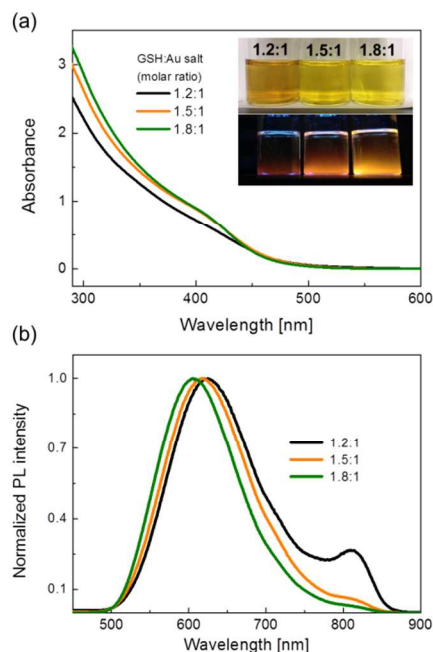


Figure 1. (a) Absorbance spectra of the synthesized gold nanoclusters with different GSH: $\text{HAuCl}_4 \cdot 3\text{H}_2\text{O}$ ratios in toluene (upper inset image is a photo of the three solutions under ambient light, and lower is under 365 nm illumination). (b) Photoluminescence spectra of the nanoclusters in toluene measured at an excitation wavelength of 365 nm.

The spectra show a small shoulder peak at a wavelength of approximately 410 nm in 1.5:1 and 1.8:1 solutions, indicating a narrower distribution of cluster size that absorb this wavelength compared to the 1.2:1 solution. Absorption onset wavelengths for these nanoclusters were located at 465-475 nm, which can be translated to approximate optical bandgaps of 2.61-2.67 eV. Photoluminescence (PL) spectra of these solutions were measured using an excitation wavelength of 365 nm, and shown in Figure 1(b). The dominant emission peaks present at wavelengths of 622 nm, 618 nm and 605 nm for the 1.2:1, 1.5:1, and 1.8:1 solutions, due to differing nanocluster size, and this slight size-dependent blue shift in emission peaks is in agreement with trends observed previously.¹⁹ Another noticeable feature in the emission spectrum of the 1.2:1 GSH: Au salt molar ratio solution is a well-resolved secondary peak at 810 nm which implies a weak bidisperse character.

To design a device structure that can efficiently facilitate charge injection into these nanoclusters, we conducted cyclic voltammetry (CV) measurements to determine their energy levels. Experiments were performed using ferrocene as a standard (CV scan results and analysis shown in Supporting Information **Figure S1** and **Figure S2**). The highest occupied molecular orbital (HOMO) levels of the nanoclusters, determined from the half potential difference between the oxidation peaks of nanoclusters and ferrocene (HOMO = 4.8 eV),²⁶ were approximately 5.25-5.28 eV. Given that the optical bandgap estimated from the absorption onset is typically smaller than the electrochemical bandgap that can be obtained from CV measurements, we were not able to explicitly derive LUMO levels out of the CV scan results due to limitations in the potential window. Judging from the previously mentioned optical bandgaps (2.61-2.67 eV), we therefore speculate that the LUMO levels are shallower than 2.6 eV. The device structure we developed has an inverted geometry, where the bottom indium tin oxide layer is used as the cathode. A ZnO electron injection layer was prepared by a sol-gel route as described in the literature,²⁷ and ultraviolet photoemission spectroscopy analysis was carried out to verify the workfunction of the ZnO layer (data shown in Supporting Information **Figure S3(a)**). The measured workfunction of the solution-processed ZnO layer is 4.2 eV, in good agreement with previously reported values, but not sufficiently low to ensure efficient electron injection into the nanocluster layer, which has an estimated LUMO level of $< 2.6 \text{ eV}$. In order to lower the workfunction further, we have utilized an ultrathin layer ($\sim 1 \text{ nm}$) of PEIE (polyethylenimine ethoxylated) on top of ZnO, resulting in a workfunction decrease of ZnO down to 3.4 eV.²⁸ Atop the PEIE layer was deposited a neat film of the metal nanoclusters. The thicknesses of ZnO and nanocluster layers were measured using variable angle spectroscopic ellipsometry and determined to be 80 nm and 8-10 nm, respectively. An 8-10 nm thick nanocluster film corresponds to roughly 5-6 layers of nanoclusters, assuming that their diameters are slightly smaller than 2 nm.¹⁹ X-ray photoemission spectroscopy was also performed on the surface of the nanocluster layer on top of ZnO, revealing Au 4f peaks from both the Au(0) nanocrystals and Au(I)-thiolate chains, along with Zn 3p peaks (Supporting Information **Figure S3(b)**), confirming the presence of a thin nanocluster layer. Subsequent layers of NPB (4,4'-bis(N-phenyl-1-naphthylamino)biphenyl) and HAT-CN (1,4,5,8,9,11-hexaazatriphenylene-hexacarbonitrile) are used as hole transport and injection layers, respectively, followed by a thick Ag layer as the

top anode. A device schematic and the corresponding energy level diagram are shown in **Figure 2**.

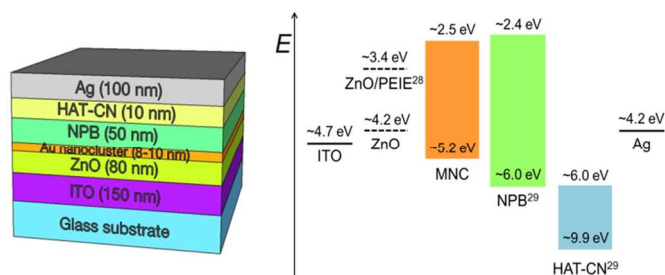


Figure 2. Device schematic and energy level diagram of the fabricated metal nanocluster based light-emitting diodes. Energy levels of certain materials were taken from literature,^{28,29} and all the values are shown with respect to the vacuum level.

Current density (J) versus voltage (V) curves of the devices incorporating the gold nanoclusters with three different GSH: Au salt ratios are shown in **Figure 3(a)**. All curves exhibit rectifying diode behavior, with varying current density levels depending on the nanocluster types. We suspect that this effect may be attributed to different amounts of Au(I)-thiolates ('surface chains' of the

nanocluster) which tune the core-shell structure size and govern charge injection and transport through the nanocluster layer. The measured forward luminance (L) versus V curves are provided in **Figure 3(b)**, with the 1.5:1 ratio nanocluster-based device showing the highest luminance, exceeding 40 cd m^{-2} , a value that is approximately two orders of magnitude greater than the earlier demonstration.²⁴ The turn-on voltages slightly varied depending on the nanocluster type, but are within a range of 2.7-3 V. In the inset of **Figure 3(b)** is a photo of a working device (1.5:1 GSH: Au salt molar ratio) in which bright orange emission originating from the nanoclusters is clearly visible. In **Figure 3(c)** are plotted the EQE of the devices versus J , wherein it can be seen that the peak EQE exceeds 0.12% for the 1.2:1 ratio device, approximately an order of magnitude larger with respect to the earlier report.²⁴ The EL spectra of the fabricated LEDs, shown in **Figure 3(d)**, additionally show that the emission originates solely from the nanoclusters rather than from parasitic regions of the device such as from an adjacent charge injection/transport layer (**Figure S3(c)**). Commission International de l'Eclairage (CIE) 1931 chromaticity coordinates (x, y coordinates) of the emission spectra of all three devices correspond to (0.57-0.59, 0.40-0.41), in the orange spectral region (Supporting Information **Figure S4**). An interesting feature emerges in the EL spectrum of the 1.2:1 ratio device, which clearly differs in shape from the PL spectrum shown in **Figure 1(b)**. While devices with 1.5:1 and 1.8:1 GSH: Au salt ratio nanoclusters exhibited almost identical EL spectra to the PL spectra with emission peak wavelengths of $\sim 625 \text{ nm}$, the

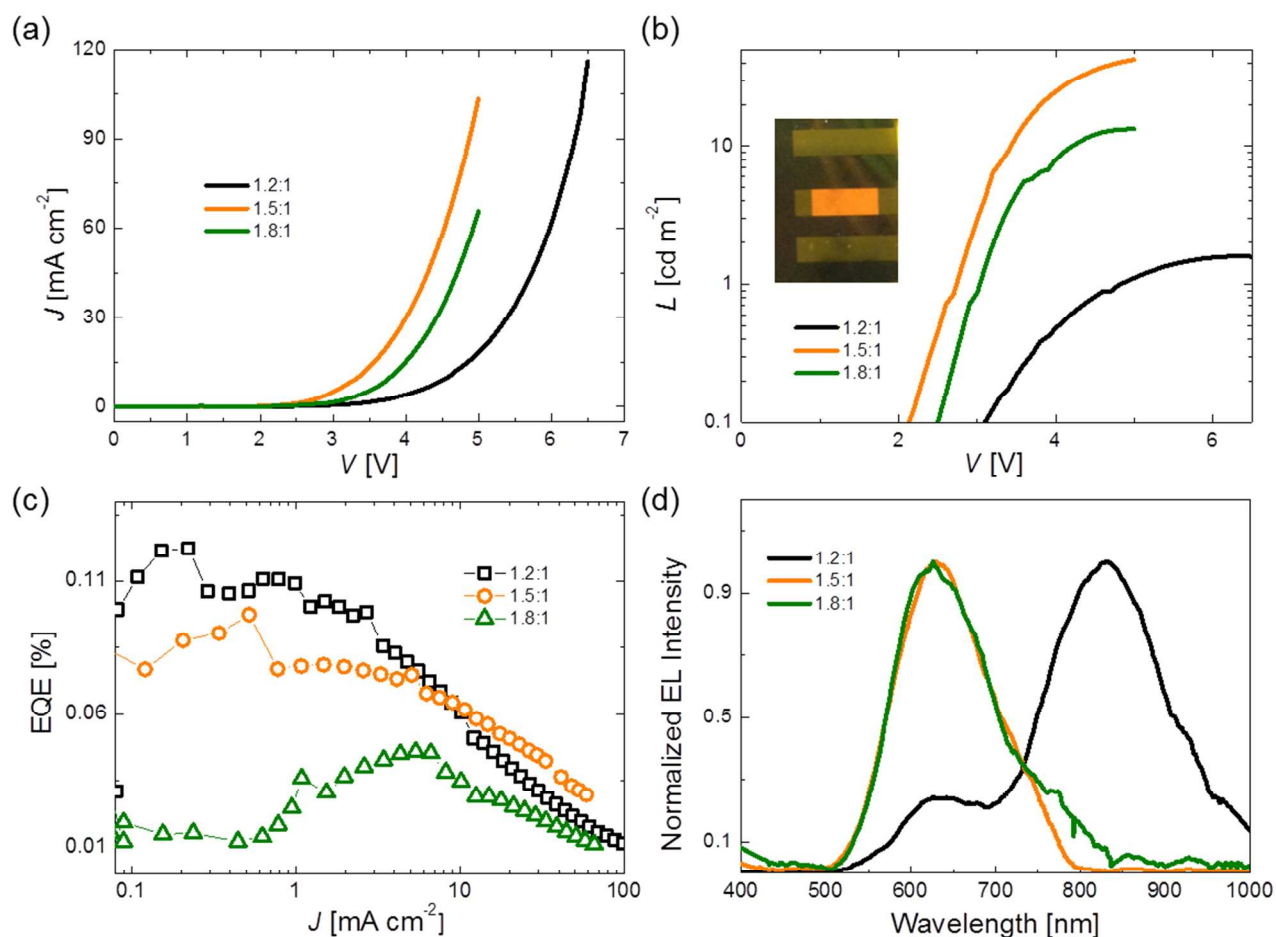


Figure 3. Optoelectronic characterization of LEDs with various Au nanocluster emitters as dictated by the synthesis with three different GSH: Au salt ratios: (a) Current density (J) versus voltage (V), (b) Forward luminance (L) versus V (inset is a photo of the 0.1 cm^2 device (1.5:1 GSH: Au salt molar ratio) under operation), (c) External quantum efficiency (EQE) versus J , and (d) Normalized electroluminescence spectra.

1.2:1 ratio device showed a dominant emission peak at a wavelength of approximately 830 nm, corresponding to the low energy, secondary emission peak in PL. Consequently, the dominant emission peak in the PL spectrum, at approximately 620 nm, became the secondary peak in the EL of the 1.2:1 device. To scrutinize this phenomenon further, we have measured the transient PL lifetime of all three types of nanoclusters in thin films.

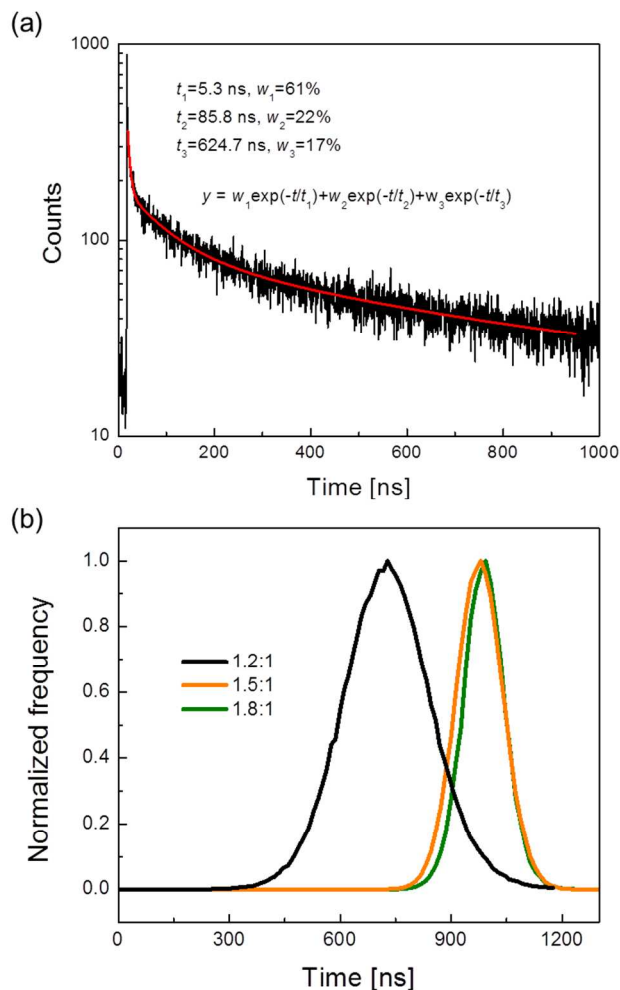


Figure 4. Transient PL lifetime measured by a fluorescence lifetime imaging microscopy (FLIM) setup. (a) Three different decay regimes were observed as shown in the legend (inset equation is the multiexponential fit with three regimes). (b) Lifetime distribution of all three types of nanoclusters. A relatively long transient lifetime of the excited states in the nanoclusters suggests that transfer of the higher energy states to lower energy states is probable in 1.2:1 nanocluster, while 1.5:1 and 1.8:1 nanoclusters are more monodispersed hence exhibit identical PL and EL spectra.

Using a fluorescence lifetime imaging microscopy (FLIM) setup, we have observed three lifetime regimes for 1.2:1 gold nanoclusters on a glass substrate, as shown in **Figure 4(a)**. A multiexponential fit reveals a fast lifetime component with $t_1 = 5.3$ ns with 61% weight, a medium regime with $t_2 = 85.8$ ns, and a long lifetime regime $t_3 = 624.7$ ns. These three regions correspond well with previously published results obtained in the solution state,¹⁹ with slight deviations possibly resulting from the increased chance of quenching between radiative sites in the film state. This relatively long transient

lifetime of the nanoclusters allows sufficient time for initially-generated, high energy excitations (in this case excitons that contribute to the ~ 620 nm emission) to be transferred to lower excited energy sites, resulting in the increased emission at longer wavelengths and a dominant EL peak at ~ 830 nm. This is further supported by the lifetime distribution measurement performed on all three types of nanoclusters in film states as shown in **Figure 4(b)**. It can be seen that the 1.2:1 nanocluster film exhibits the shortest transient lifetime distribution among the three whereas the other two types show average lifetimes of approximately 1 μ s. Furthermore, the 1.2:1 nanoclusters were the only type to exhibit a noticeable bidisperse size distribution according to the PL, as shown in Fig. 1(b). Therefore this discrepancy between the EL and PL spectrum is most pronounced in the 1.2:1 nanocluster layer, where, owing to the long lifetime, energy transfer from excitons generated in larger nanoclusters to smaller nanoclusters is able to take place. Though not as prominent as the case of the 1.2:1 nanocluster layer, this phenomenon can also be observed in 1.5:1 and 1.8:1 nanocluster layers; almost identical EL peaks of 1.5:1 and 1.8:1 devices near 620 nm are slightly red-shifted compared to the PL peak of 1.8:1 (605 nm) but are similar to that of 1.5:1 (618 nm), hence further supporting our argument. This also indicates that the EL mechanism from this aggregation-induced emission type of nanoclusters was not because of a quantum confinement effect within the nanoclusters as in the case of quantum dots, but due to ligand-to-metal or ligand-to-metal-metal charge transfer¹⁹ as in the case of molecular emitters while the emission properties are still governed by the interplay of the core/shell and their overall size. The low forward luminance of the 1.2:1 ratio nanocluster-based LED, despite its higher peak EQE compared to the other ratios, is understood from the fact that the dominant emission peak is situated in the infrared region, invisible to the human eye. It is furthermore an intriguing example of preparing active emitters in different spectral ranges that share a similar synthetic protocol, which could be further expanded not only by changing the size of the nanoclusters but also by changing the metal and ligands themselves.^{20,30}

Finally, the large shifts between absorption and emission spectra (~ 200 nm) and relatively long radiative decay lifetime approaching the microsecond range are indirect evidence of triplet emission. In the case of QD-LEDs, the use of a neat layer has proven highly effective to demonstrate highly efficient devices,¹¹ owing to a short excited state lifetime in the ns range.³¹ Hence, in the case of metal nanocluster LEDs, there is a need to develop a device structure that can mitigate the likelihood of quenching between the long-lived triplet excited states, for example a host:guest emissive layer that is able to maintain separation between nanoclusters, an aspect which is currently under investigation. Also, further efficiency enhancement can be achieved in other ways such as the incorporation of luminescent nanoclusters with higher PLQY and shorter-lived excited states, through modification of core and surface ligands that affect both optical (e.g. emission spectrum) and electrical (e.g. charge injection and transport) properties of the nanoclusters.

Conclusions

To summarize, we have adopted a simple one-pot synthetic protocol for preparing luminescent gold nanoclusters to fabricate Au(0)@Au(I)-thiolate nanoclusters with various sizes and hence different photophysical properties, and incorporated them as active emitters in thin film light-emitting devices. Based on the energy levels of the nanoclusters obtained from cyclic voltammetry and optical absorption measurements, we have designed and fabricated inverted structure thin film LEDs

that exhibited a peak external quantum efficiency greater than 0.1%, an order of magnitude enhancement compared to the initial demonstration of the metal nanocluster LED,²⁴ and a peak luminance exceeding 40 cd m⁻² which was a more than two orders of magnitude improvement with fully suppressed parasitic emission. A noticeable difference between the EL and PL spectra of the LED with the smallest nanoclusters has been observed, which was explained by the long transient PL lifetime of the nanoclusters, suggesting ways in which metal nanocluster LEDs can be engineered for increased performance.

Experimental methods

Synthesis of the gold nanoclusters: All chemicals sourced from commercially available vendors and were used without further purification. Reduced L-Glutathione (GSH, Sigma Aldrich) and hydrogen tetrachloroaurate trihydrate (HAuCl₄·3H₂O, Alfa Aesar) were dissolved in deionized water at 100 mM and 20 mM concentrations respectively. 0.12/0.15/0.18 ml of aqueous GSH solutions and 0.5 ml of aqueous Au salt solution were added to 4.35 ml of deionized water, and the mixtures were stirred at 300 rpm on a hotplate at 75 °C for 80 hours. (Each noted as 1.2:1, 1.5:1, 1.8:1 ratio solutions based on molar ratios) After synthesis, solutions were neutralized to pH of 7-8 by adding small amounts of aqueous NaOH, and filtered using 0.02 μm pore size syringe filters (Anotop, Whatman). For phase transfer into organic solvents (DCM (dichloromethane) for cyclic voltammetry measurement / toluene for device fabrication), 5 ml of ethanol with CTAB (hexadecyltrimethyl ammonium bromide, Sigma Aldrich) dissolved at 100 mM was added to the aqueous solution and vigorously stirred. Then DCM or toluene was added to the solution and stirred well, initiating phase transfer of the nanoclusters that completed within minutes.

Cyclic voltammetry measurements: Tetrabutylammonium hexafluorophosphate (500 mg) was dissolved in 10 ml of anhydrous DCM as the electrolyte. Nanoclusters in DCM (15 ml of aqueous phase nanoclusters transferred into 3 ml of DCM) were added to the solution, together with 3 mg of ferrocene (Sigma Aldrich) as a standard. Glassy carbon, non-aqueous Ag/Ag⁺, and platinum wire electrodes were used as working, reference and counter electrodes, respectively, to perform cyclic voltammetry scans using a CHI660C electrochemical analyzer (CH Instruments, Inc.), at a scan rate of 50 mV s⁻¹. Both oxidation/reduction scans were performed in a complete single cycle, and the scans were performed after the addition of each material (i.e. electrolyte, nanoclusters, ferrocene) to the DCM solvent, and the cycles were repeated at least 3 times to verify the consistency between them and to rule out possible ongoing chemical reaction.

Nanocluster characterization and device fabrication/analysis: Photoluminescence spectra of the synthesized nanoclusters in toluene were obtained using an F-7000 fluorescence spectrophotometer (Hitachi High-Tech) with quartz cuvettes, and absorbance spectra were measured using Cary 500 UV-VIS-NIR spectrophotometer (Varian). For device fabrication,

patterned ITO substrates were cleaned using soapy water, DI water, acetone and isopropanol in sequence using an ultrasonicator, and ZnO solution was spincoated at 2000 rpm and baked at 200 °C in air for 10 min on a hotplate (ZnO solution preparation described elsewhere²³). Polyethylenimine ethoxylated (PEIE) diluted at 0.1 wt% in 2-methoxyethanol was spincoated on the ZnO layer at a spin speed of 5000 rpm, and the substrates were baked again in air at 150 °C for 15 min on a hotplate. After the final spincoating of nanoclusters dispersed in toluene at 600 rpm, samples were brought into a vacuum thermal evaporation chamber (EvoVac, Angstrom Engineering) for subsequent depositions of 50 nm of NPB (4,4'-bis(N-phenyl-1-naphthylamino)biphenyl, Nichem), 10 nm of HAT-CN (1,4,5,8,9,11-hexaazatriphenylene-hexacarbonitrile, Nichem), and 100 nm of Ag (R. D. Mathis) defining devices with area of 0.1 cm². Completed devices were analyzed using a homemade motorized goniometer setup connected to a Keithley 2400 sourcemeter unit, a calibrated Si photodiode (FDS-100-CAL, Thorlabs), and a picoammeter (4140B, Agilent). Electroluminescence spectra were measured using a calibrated fiber optic spectrophotometer (UVN-SR, StellarNet Inc.).

Transient PL lifetime measurement: Fluorescence lifetime imaging microscopy measurements were carried out on an inverted confocal microscope (Oxford X71) coupled to a diode pumped solid state laser delivering 440 nm, 90 ps pulses, at 8 MHz repetition rate. The sample luminescence was spectrally separated from the laser by a Semrock RazorEdge 532 long pass filter (LPF) and detected by an MPD Picoquant Avalanche Photodiode (APD) coupled to a PicoHarp 300 time analyzer. See Supporting Information Figure S5 for a simplified schematic of the setup. Laser spot size on the sample was 0.5×0.5×2 μm and the pinhole placed before the APD had a diameter of 75 μm. A 60X air objective with NA 0.85 was used for all measurements.

Notes and references

^a Department of Electrical Engineering, Princeton University, Princeton, New Jersey 08544, United States

^b Department of Chemical and Biological Engineering, Princeton University, Princeton, New Jersey 08544, United States

^c Department of Physics, City College, City University of New York, New York 10031, United States

^d Department of Physics, Princeton University, Princeton, New Jersey 08544, United States

^e Andlinger Center for Energy and the Environment, Princeton University Princeton, New Jersey 08544, United States

† Electronic Supplementary Information (ESI) available: See DOI: 10.1039/c000000x/

- Z. B. Wang, M. G. Helander, J. Qiu, D. P.uzzo, M. T. Greiner, Z. M. Hudson, S. Wang, Z. W. Liu, Z. H. Lu, Z. H. *Nature Photon.* 2011, **5**, 753-757.
- S. Kim, H. -J. Kwon, S. Lee, H. Shim, Y. Chun, W. Choi, J. Kwack, D. Han, M. S. Song, S. Kim, S. Mohammadi, I. S. Kee, S. Y. Lee, *Adv. Mater.* 2011, **23**, 3511-3516.

- 3 H. Cho, J. Choi, S. Yoo, *Opt. Express* 2011, **19**, 1113-1121.
- 4 J. -S. Yoo, S. -H. Jung, Y. -C. Kim, S. -C. Byun, J. -M. Kim, N. -B. Choi, S. -Y. Yoon, C. -D. Kim, Y. -K. Hwang, I. -J. Chung, *J. Disp. Tech.* 2010, **6**, 565-570.
- 5 A. Sugimoto, H. Ochi, S. Fujimura, A. Yoshida, T. Miyadera, M. Tsuchida, *IEEE J. Sel. Topics Quantum Electron.* 2004, **10**, 107-114.
- 6 D. -Y. Yoon, T. -Y. Kim, D. -G. Moon, *Curr. Appl. Phys.* 2010, **10**, e135-e138.
- 7 Y. Kawamura, K. Goushi, J. Brooks, J. J. Brown, H. Sasabe, C. Adachi, *Appl. Phys. Lett.* 2005, **86**, 071104-071104-3.
- 8 S. O. Jeon, S. E. Jang, H. S. Son, J. Y. Lee, *Adv. Mater.* 2011, **23**, 1436-1441.
- 9 C. -L. Ho, W. -Y. Wong, Z. -Q. Gao, C. -H. Chen, K. -W. Cheah, B. Yao, Z. -Y. Xie, Q. Wang, D. -G. Ma, L. -X. Wang, X. -M. Yu, H. -S. Kwok, Z. -Y. Lin, Z. -Y. *Adv. Funct. Mater.* 2008, **18**, 319-331.
- 10 K. P. Klubek, C. W. Tang, L. J. Rothberg, *Org. Electron.* 2014, **15**, 1312-1316.
- 11 B. S. Mashford, M. Stevenson, Z. Popovic, C. Hamilton, Z. Zhou, C. Breen, J. S. Steckel, V. Bulović, M. Bawendi, S. Coe-Sullivan, P. T. Kazlas, *Nature Photon.* 2013, **7**, 407-412.
- 12 X. Dai, Z. Zhang, Y. Jin, Y. Niu, H. Cao, X. Liang, L. Chen, J. Wang, X. Peng, *Nature* 2014, **515**, 96-99.
- 13 J. S. Steckel, P. Snee, S. Coe-Sullivan, J. P. Zimmer, J. E. Halpert, P. Anikeeva, L. -A. Kim, V. Bulović, M. G. Bawendi, *Angew. Chem. Int. Ed.* 2006, **45**, 5796-5799.
- 14 D. J. Norris, M. G. Bawendi, *Phys. Rev. B.* 1996, **53**, 16338.
- 15 P. O. Anikeeva, J. E. Halpert, M. G. Bawendi, V. Bulović, *Nano Lett.* 2009, **9**, 2532-2536.
- 16 I. Gur, N. A. Fromer, M. L. Geier, A. P. Alivisatos, *Science* 2005, **310**, 462-465.
- 17 I. J. Kramer, E. H. Sargent, *ACS Nano*, 2011, **5**, 8506-8514.
- 18 R. Hardman, *Environ. Health Persp.* 2006, **114**, 165-172.
- 19 Z. Luo, X. Yuan, Y. Yu, Q. Zhang, D. T. Leong, J. Y. Lee, J. Xie, *J. Am. Chem. Soc.* 2012, **134**, 16662-16670.
- 20 X. Yuan, Z. Luo, Q. Zhang, X. Zhang, Y. Zheng, J. Y. Lee, J. Xie, *ACS Nano*, 2011, **5**, 8800-8808.
- 21 J. Zheng, C. Zhang, R. M. Dickson, *Phys. Rev. Lett.* 2004, **93**, 077402.
- 22 L. Shang, S. Dong, G. U. Nienhaus, *Nanotoday*, 2011, **6**, 401-408.
- 23 J. A. Ho, H. -C. Chang, W. -T. Su, *Anal. Chem.* 2012, **84**, 3246-3253.
- 24 B. Niesen, B. P. Rand, *Adv. Mater.* 2014, **26**, 1446-1449.
- 25 S. Wang, X. Meng, A. Das, T. Li, Y. Song, T. Cao, X. Zhu, M. Zhu, R. Jin, *Angew. Chem. Int. Ed.* 2014, **53**, 2376-2380.
- 26 J. Pommerehne, H. Vestweber, W. Guss, R. F. Mahrt, H. Bässler, M. Porsch, J. Daub, *Adv. Mater.* 2004, **7**, 551-554.
- 27 Y. Sun, J. H. Seo, C. J. Takacs, J. Seifert, A. J. Heeger, *Adv. Mater.* 2011, **23**, 1679-1683.
- 28 Y. Zhou, C. F. Hernandez, J. Shim, J. Meyer, A. J. Giordano, H. Li, P. Winget, T. Papadopoulos, H. Cheun, J. Kim, M. Fenoll, A. Dindar, W. Haske, E. Najafabadi, T. M. Kahn, H. Sojoudi, S. Barlow, S. Graham, J. -L. Brédas, S. R. Marder, A. Kahn, B. Kippelen, *Science*, 2012, **336**, 327-332.
- 29 Y. -K. Kim, J. W. Kim, S. Park, *Appl. Phys. Lett.* 2009, **94**, 063305.
- 30 Z. Wu, R. Jin, *Nano Lett.* 2010, **10**, 2568-2573.
- 31 Y. Shirasaki, G. J. Supran, W. A. Tisdale, V. Bulović, *Phys. Rev. Lett.* 2013, **110**, 21703.